Biophysical Journal, Volume *112*

Supplemental Information

Interdigitation between Triglycerides and Lipids Modulates Surface Properties of Lipid Droplets

Amélie Bacle, Romain Gautier, Catherine L. Jackson, Patrick F.J. Fuchs, and Stefano Vanni

Supporting Information

to the article

Interdigitation between core triglycerides and surface phospholipids modulates the surface properties of lipid droplets.

A. Bacle, R. Gautier, C. Jackson, P. Fuchs and S. Vanni

Supplementary methods

United-atom simulations – System preparation

For convenience, Table 1 of the main text is reproduced here as Table S1, it describes the different united-atom systems we simulated:

System	Time (ns)	# TO	# POPC	# waters	acronym
pure TO	150	108	-	-	pureTO
TO / vacuum	200	108	-	-	TO/vac
TO / water	200	108	-	5292	TO/W
POPC bilayer NPT	300	-	200	7943	POPCbil
LD NPT	300	204	200	7941	LD0
LD NPT 4x surface	300	816	800	31764	LD0-4x
LD 1% area increase	300	204	200	7929	LD1
LD 2% area increase	300	204	200	7924	LD2
LD 5% area increase	300	204	200	7915	LD5
LD 10% area increase	300	204	200	7903	LD10

Table S1. **List of all-atom simulations described in the text.** Surface tensions (ST) are described in this table as percentage of increase with respect to the area of a bilayer (with the same number of POPC) at equilibrium (thus at 0 surface tension). The corresponding values of ST in units of mN/m are given in Table 2 in the main text. A snapshot of the LD0 system is presented in Figure 1 in the main text.

The pure TO system (pureTO, consisting of 108 TO molecules) was initially obtained from Ilpo Vatulainen (35) and a pure POPC bilayer from the Tieleman web site (http://wcm.ucalgary.ca/tieleman/downloads). This latter bilayer was expanded in order to get 100 POPC per monolayer (POPCbil). The construction of the trilayer systems at 0 surface tension (LD0) required a few more steps. The initial pureTO system was expanded to 204 TO molecules in order to get approximately the same *xy* dimensions as the POPCbil system (~ 66 nm^2). Then, the two POPC monolayers were separated in the *z* direction and the box of 204 TO was placed in between them. After system hydration (and careful removing of waters trapped in POPC and TO), box edges were adapted around the final system and periodic boundary conditions (PBC) recovered by successive minimizations. To obtain trilayer systems under positive surface tension, the *xy* dimensions of the LD0 system were progressively

increased by small steps and the system minimized at each step; at the end, we obtained systems with a 1, 2, 5 and 10% of total area increase with respect to that of LD0 and we simulated them keeping the *xy* area constant. Note that this way of proceeding can lead to different surface tension values when simulating the same system (with the same total *xy* area) with different initial conditions (see below).

For the TO/water (TO/W) and TO/vacuum (TO/vac) interfaces, the systems were constructed from the pureTO system by expanding the *z* direction and hydrating or not the layers of vacuum. After all these construction steps, each system was properly minimized and equilibrated for a few tens of ns by MD with the Berendsen thermostat and barostat(37).

United-atom simulations – Simulation details

United-atom simulations (UA) were performed with GROMACS 4(1) using the Berger force field for POPC phospholipids(2) and the SPC water model (3). For trioleins (TO, tri-C18:1) the parameters adapted from Berger by Vattulainen and co-workers were used (4) (starting from a POPC molecule, the *sn*-3 was replaced by an oleoyl chain). For all oleoyl chains (POPC and TO), the correction on the double bond of (5) was applied. Several systems were constructed and are described in Table S1.
Pressure control was adapted in each case: isotropically in all dimensions for the pureTO system (NPT), semi-isotropically (*xy* scaled together, *z* scaled independently) for the systems at equilibrium (POPCbil and LD0) (NPT), only in the *z* dimension for trilayer systems under positive surface tension (LD1, LD2, LD5 and LD10) as well as for the TO/W interface (NP_zAT because we keep the *xy* area constant). No pressure was applied for the TO/vac interface (NVT).
Production runs of several hundreds of ns were done at 300K using the velocity-rescaling thermostat of Bussi(6) (time constant of 0.1 ps, POPC/TO/water coupled separately) and at 1 bar (when applicable) using the Parrinello-Rahman barostat(7) (time constant of 4 ps and a compressibility of 4.5×10^{-5} bar^{-1}). Bond lengths were constrained using the P-LINCS algorithm(1). A time step of 2 fs was used with the leap-frog integrator. Water molecules were kept rigid using the SETTLE algorithm(8). A cutoff of 1.0 nm was used for Lennard-Jones interactions. The smooth particle-mesh-Ewald (PME) method(9, 10) was used for electrostatic interactions (with a real space cutoff of 1.0 nm, a grid of 0.12 nm^{-1} and an interpolation order of 4). The neighbour list was updated every 10 steps.

United-atom simulations – Analyses

Frames were saved every 100 ps and trajectory analyses were performed on the last 200 ns for each simulation (the first 100 ns were systematically discarded from the analysis). All simulations were performed twice (or three times for LD10) and divided into 3 blocks. Except otherwise stated, final results are presented as an average over 6 blocks (3 blocks times 2 trajectories), and the error is the corresponding standard deviation. All molecular graphics were generated with VMD (1). We describe in the following the details of each analysis we performed, in the same order as they appear in the main manuscript.

Area per lipid

The area per lipid was calculated as the area of the lateral *xy* dimension of the box divided by the number of lipids per leaflet. For LD systems under positive ST, the area is fixed, thus it has no fluctuation.

Surface tension

For all simulations, surface tension was computed from the diagonal values of the pressure tensor (P_{xx}, P_{yy} and P_{zz}) using the Kirkwood-Irving method(2) :

$$\gamma \approx \frac{L}{2}\left\langle P_{zz} - \frac{P_{xx}+P_{yy}}{2}\right\rangle \qquad (1),$$

where L is the box length in the z dimension and $\langle ... \rangle$ means an ensemble average. Notice that because of high fluctuations in P_{xx}, P_{yy} and P_{zz}, γ fluctuates vigorously on a microscopic system of a few thousands of atoms such as ours. Thus two simulations of the same system with constant *xy* total area but with different initial velocities can lead to different values of γ on the hundreds of ns timescale. For this reason, the average and error on γ were evaluated from the *g_energy* GROMACS tool (*g_energy* outputs to the screen average and error using points at all time steps, which is more precise than generating an xvg file and doing the analysis on the latter) using the whole trajectory for each simulation. Error was evaluated using a block averaging procedure with 5 blocks. Average and error are reported in Table S12 for each individual simulation. In Table 1 of the main manuscript, we report a single value for each system, which was obtained by concatenating all trajectories of a given system prior to the procedure with *g_energy*. When the error is not indicated in Table 1 or Table S12, it is below 0.1 mN/m.

Last, γ is called interchangeably surface tension or interfacial tension in this paper.

Monolayer Thickness

Monolayer thickness was calculated from a density plot using the peak-to-peak distance between the first and last aliphatic carbon atoms of the sn-1 chain of the POPC lipids.

Lateral diffusion

Lateral diffusion of POPC molecules (considering phosphorous atoms of POPC) was calculated from the slope of the mean square displacement curve using Einstein law. To correct for the overall motion of each monolayer, the linear momentum was removed at each step for each monolayer separately (2). The trajectory was divided into two blocks. The final value and error reported in Table 1 (of the main manuscript) is an average and standard deviation over the two trajectories and two leaflets (four values).

Order parameter

The order parameter was calculated as described in ref (3). Since we used a united-atom force field, we first reconstructed the hydrogens using the *g_protonate* tool of GROMACS. The order parameter S_{CH} was then calculated using:

$$S_{CH} = \frac{1}{2}\left\langle 3\cos^2\theta - 1 \right\rangle \qquad (2),$$

where θ is the angle between the C-H bond and the membrane normal, and $\langle ... \rangle$ means an ensemble average. In Table 1 of the main manuscript, we report the order parameter of a few carbon atoms of the *sn*-2 (unsaturated) chain: i) the first aliphatic carbon atom (start), ii) the carbon atom just before the double bond (middle) and iii) the last one of the chain (end). Errors on order parameter were systematically below 0.02 and are thus not reported in this table.

Lateral pressure profile

Lateral pressure profiles (LPPs) $\pi(z)$ were evaluated for the LD0, TO/W and POPCbil systems:

$$\pi(z) = P_L(z) - P_N \qquad (5),$$

where $P_L(z)$ is the lateral component of the pressure tensor ($P_L(z) = \frac{1}{2}\,(P_{xx}(z) + P_{yy}(z))$) and P_N the normal component ($P_N = P_{zz}$). Note that the integral of $\pi(z)$ is directly related to the negative of γ:

$$\int_0^L \pi(z)dz = -\gamma \qquad (6),$$

where L is the box size in the z dimension. A negative $\pi(z)$ means the system wants to shrink the lateral dimension, a positive $\pi(z)$ means the system wants to expand the lateral dimension. When the area of the system is at equilibrium, negative and positive contributions to $\pi(z)$ cancel out and $\gamma = 0$. Note here that the definition of the 0 for the z axis in the integral of equation (6) does not matter (the bilayer does not need to be centered). In this work, all UA LPPs were computed using the program GROMACS-LS obtained at http://mdstress.org/ (4). A grid of 1 Å in the z dimension was used, and LPP were obtained by performing a rerun on a window of 100 ns (one frame every 5 ps) after 400 ns of equilibration and using a cutoff of 22 Å for electrostatics.

GROMACS-LS allows computing the LPP using both central force decomposition (CFD) and Goetz-Lipowsky decomposition (GLD). CFD has been shown (4) to handle correctly the constraints in contrast to GLD. However, the LPPs computed from the CG simulations (see below) where obtained using another MD code (LAMMPS) for which only GLD is implemented. We thus decided to report in Figure S6 a comparison of LPPs of 3 systems (namely LD0, POPCbil and TO/W) using both decompositions. Overall, the shape is the same

with only a few differences in the magnitude of peak III, that represents the acyl chains towards the oil/bilayer interior. Importantly, this does not change the comments and conclusions of Figure 2 of the main manuscript. In order to be consistent in the different LPPs presented in this article (UA (Figure 2) / CG (Figures 6 and 8)), we report in Figure 2 the LPP using the GLD decomposition.
Interestingly, the first moment of the LPP is directly related to the curvature properties of a bilayer, namely the free energy derivative with respect to total curvature ($\overline{F}'$) at 0 curvature $\overline{F}'(0)$ (5) :

$$\overline{F}'(0) = -\int_{-\infty}^{+\infty} z\pi(z)dz \qquad (7),$$

where the bar means $\overline{F}'(0)$ is expressed per unit lipid area. Here z = 0 is set at the middle of the bilayer. For a planar symmetric bilayer, $\overline{F}'(0)$ is 0 with the top and bottom leaflets having opposite signs (a non 0 $\overline{F}'(0)$ means that the bilayer would spontaneously bend).

Alternatively, according to Helfrich theory(6), the membrane energy per unit-area can be written as(7):

$$\overline{F} = \frac{k_c}{2}\left(c_1 + c_2 - c_0\right)^2 + k_g c_1 c_2 \qquad (8),$$

where c_1 and c_2 are the two principal curvatures, c_0 is the spontaneous curvature, and k_c and k_g are, respectively, the bending and Gaussian moduli.

The first derivative of the free energy with respect to total curvature, evaluated at zero curvature, thus becomes:

$$\overline{F}'(0) = -k_c c_0 \qquad (9)$$

Defining $\overline{F}'(0)$ on a leaflet basis is useful because it is directly related to the negative of the product bending modulus (k_c) times the spontaneous curvature (c_0) (that is also defined on a leaflet basis(7)):

$$\overline{F}'(0) = -\int_{0}^{L/2} z\pi(z)dz = -k_c c_0 \qquad (10)$$

where L is the box size in the z axis (again z = 0 is set at the middle of the bilayer).

Computing the LPP from a computer simulation of a planar bilayer (or planar trilayer system for LD) thus allows the extraction of c_0, or at least the sign of c_0 if k_c is unknown (as in our case), directly from $\overline{F}'(0)$. A positive sign of c_0 implies the monolayer would bend convexly (with a larger area for the polar heads), a negative sign means it would bend concavely (with more area for the aliphatic tails). To be able to compare $\overline{F}'(0)$ for a POPC bilayer and a LD system, we followed this procedure: i) first we set z = 0 (the middle of the bilayer) on the LPP of POPC by taking the exact center between the two big negative peaks, ii) we aligned the (right) big negative peak of LD LPP with the right one of POPC, iii) we performed the

integration only for positive *z* values. This is a valid procedure since the thickness of POPC monolayer is barely affected by the presence of oil (see Table 2 of the main text).

Coarse-grained simulations – MARTINI simulations

MARTINI simulations were performed using the software GROMACS 4(8), with POPC parameters taken from version 2.0 of the lipid force field (with 5 beads in the oleoyl tail) and triolein (TO) parameters taken from reference(9). Non-bonded interactions (electrostatics and Lennard-Jones) were treated using shifted potentials with a cut-off radius of 1.2 nm. Temperature was kept at 300K using the velocity rescale thermostat by Bussi et al(10), while pressure was controlled separately (semi-isotropic) at 1 atm for the *xy* and *z* coordinates through the coupling to an external bath using the Berendsen algorithm(11). For simulations at non-zero surface tension (TO/W system) the *x* and *y* dimensions were fixed and pressure was controlled only along the *z* coordinate. In all systems, a time step of 30 fs was used. No time conversion factor was used to estimate the length of all production and equilibration runs.
All CG systems are summarized in Table S2. The pure TO system was obtained by self-assembly of a random mixture of TO molecules, while the LD-mimicking model systems were obtained by placing two pre-equilibrated POPC monolayers at the two sides of the pure TO system. 14150 water molecules were added such as to keep the two POPC monolayers at a distance larger than 2 times the cut-off distance (2 × 1.2 nm).

Force field	System	Time (ns)	# TO	# POPC	# waters
MARTINI	pure TO	90	400	-	-
MARTINI	TO/W	90	108	-	5292
MARTINI	LD NPT	900	1250	1000	14150
MARTINI	LD NPT “UA-size”	900	204	200	4353
SDK & this work	pure TO	500	108	-	-
SDK & this work	TO/air	400	204	-	-
SDK & this work	TO/W	500	108	-	1764
SDK & this work	POPC bilayer	800	-	288	4800
SDK & this work	POPC bilayer 4x surface	800	-	1152	14661
SDK & this work	LD NPT “UA-size”	500	204	200	3845
SDK & this work	LD NPT 1z	500	816	800	15380
SDK & this work	LD NPT 2z	500	1632	800	15363
SDK & this work	LD NPT 3z	500	2448	800	15363
SDK & this work	LD 2z – 400 POPC	500	1632	800	15363
SDK & this work	LD 2z – 396 POPC	500	1632	792	15363
SDK & this work	LD 2z – 394 POPC	500	1632	788	15363
SDK & this work	LD 2z – 392 POPC	500	1632	784	15363
SDK & this work	LD 2z – 390 POPC	500	1632	780	15363

SDK & this work	LD 2z – 388 POPC	500	1632	776	15363
SDK & this work	LD 2z – 386 POPC	500	1632	772	15363
SDK & this work	LD 2z – 384 POPC	500	1632	768	15363
SDK & this work	LD 2z – 382 POPC	500	1632	764	15363
SDK & this work	LD 2z – 380 POPC	500	1632	760	15363
SDK & this work	LD 2z – 378 POPC	500	1632	756	15363
SDK & this work	LD 2z – 376 POPC	500	1632	752	15363
SDK & this work	LD 2z – 374 POPC	500	1632	748	15363
SDK & this work	LD 2z – 372 POPC	500	1632	744	15363
SDK & this work	LD 2z – 370 POPC	500	1632	740	15363
SDK & this work	LD 2z – 368 POPC	500	1632	736	15363
SDK & this work	LD 2z – 364 POPC	500	1632	728	15363
SDK & this work	LD 2z – 360 POPC	500	1632	720	15363
SDK & this work	LD 2z – 352 POPC	500	1632	704	15363
SDK & this work	LD 2z – 344 POPC	500	1632	688	15363
SDK & this work	LD 2z – 336 POPC	500	1632	672	15363
SDK & this work	LD 2z – 328 POPC	500	1632	656	15363
SDK & this work	LD 2z – 320 POPC	500	1632	640	15363
SDK & this work	LD 2z – 280 POPC	500	1632	560	15363
SDK & this work	LD 2z – 240 POPC	500	1632	480	15363
SDK & this work	LD 2z – 200 POPC	500	1632	400	15363
SDK & this work	LD 2z – 140 POPC	500	1632	280	15363
SDK & this work	TO/W 2z	500	408	0	3841

Table S2. List of CG simulations described in the text.

Coarse-grained simulations – Derivation of CG TO parameters based on the SDK model

We also used the CG lipid model by Klein and coworkers(12, 13) as basis to derive additional TO parameters, following the procedure by Shinoda *et al*. (14). First, a natural UA to CG mapping, consistent with that of the existing phospholipids(12), was defined (see Figure S4). Second, parameters for the oleoyl chains were kept identical to those in phospholipids. Third, new bonded parameters (angles, bonds) for the interactions involving the three new beads describing the glycerol (GLT), the central (ESTC, position 2) and the lateral (ESTL, positions 1 and 3) esters of TO were obtained following the Shinoda-DeVane-Klein (SDK) parameterization procedure(14), *i.e*. by targeting average and standard deviation of the corresponding bond and angular probability distribution obtained from the UA simulations of pure TO systems described above. Fourth, all non-bonded parameters for the new groups were kept identical to those in phospholipids, using the parameters for glycerol for GLT and those of esters for ESTC and ESTL, with the sole exception of the parameters for the interaction between the new glycerol bead and water beads (GLT-W), that was modified in order to

reproduce correctly the triolein-water interfacial tension of 32 mN/m (15). Fifth, angular parameters were further refined to better reproduce the distribution of TO conformations. In particular, since "Fork" conformations were severely underestimated before this optimization step, the angular parameters were modified such as to increase this specific population by targeting the UA angular distribution of this specific population as opposed to that of all TO molecules. All new parameters for TO molecules are available in Figure S4.

Coarse-grained simulations – System preparation

Configurations for the CG systems were generated by converting atomistic snapshots using the CG-it software (https://github.com/CG-it) and simulations were performed with LAMMPS (16).
LD-mimicking systems with this force field were initially mapped from the corresponding UA simulations described above and consisted of 204 TO molecules and 200 POPC molecules (100 phospholipids per leaflet). The pure TO system consisted of 108 TO molecules without phospholipids. These systems were used to optimize the CG parameters and to directly compare the TO conformations with UA simulations. Next, larger CG systems were used to compute the Π-A isotherm, lipid-packing defects and lateral pressure profiles. All systems are summarized in Table S2.
CG simulations for POPC bilayers were started from atomistic snapshots obtained using the membrane builder of CHARMM-GUI(17) after mapping to CG resolution.

Coarse-grained simulations – Simulation details

In LAMMPS, pressure and temperature were controlled using a Nosé-Hoover thermostat(18) and barostat(19, 20), with target temperature and pressure of 300 K and 1 atm, respectively. With the exception of pure TO simulations, the lateral *xy* dimensions of the LD system were constrained to be equal, while the orthogonal dimension *z* was allowed to fluctuate independently. For simulations at non-zero surface tension, the *xy* lateral dimensions were kept fixed. Van der Waals and electrostatics were truncated at 1.5 nm, with long-range electrostatics beyond this cutoff computed using the particle-particle-particle-mesh (PPPM) solver with an RMS force error of 10^{-5} kcal mol^{-1} $Å^{-1}$ and order 3(21). In all simulations with this CG model, a time step of 20 fs was used.

Coarse-grained simulations – Analyses

For all simulations, surface tension was computed as described above for UA simulations using the Kirkwood-Irving method(2). Lipid-packing defects were computed using a previously described algorithm(22, 23) while taking into account TO molecules only if at least one of their atoms was above the imposed threshold along the normal to the membrane. For the CG model, the bead size was taken from the diagonal σ values σ_{ii} for every bead type, and the glycerol level was computed from the average z position of the "GL" beads (that map the three carbon atoms of the glycerol groups) of the POPC molecules. The threshold for deep lipid-packing defects was set at 0.2 nm below the glycerol level.
The same conformational analysis of TO molecules described for the UA simulations was performed for the CG simulations. To define the optimal beads to identify the chain unit vectors in the CG representations, we computed the distribution of TO molecules in UA trajectories directly mapped to CG for all possible vectors composing the various acyl chains (see Supplementary Table S5). For the CG analysis, we selected the vector (C1-C2) that

provided the best agreement with the UA analysis (C1-C2, with an average relative error of 5%).
All analyses were performed on the last 400 ns of simulations, with the exception of lateral pressure profiles that were computed on the last 200 ns of trajectory as in (24), with a grid resolution of 1 Å.

Supporting references.

1. Humphrey, W., A. Dalke, and K. Schulten. 1996. VMD: visual molecular dynamics. J Mol Graph 14:33-38, 27-38.
2. Irving, J. H., and J. G. Kirkwood. 1950. The Statistical Mechanical Theory of Transport Processes. IV. The Equations of Hydrodynamics. The Journal of Chemical Physics 18:817-829.
3. Botan, A., F. Favela-Rosales, P. F. Fuchs, M. Javanainen, M. Kanduc, W. Kulig, A. Lamberg, C. Loison, A. Lyubartsev, M. S. Miettinen, L. Monticelli, J. Maatta, O. H. Ollila, M. Retegan, T. Rog, H. Santuz, and J. Tynkkynen. 2015. Toward Atomistic Resolution Structure of Phosphatidylcholine Headgroup and Glycerol Backbone at Different Ambient Conditions. The journal of physical chemistry. B 119:15075-15088.
4. Vanegas, J. M., A. Torres-Sanchez, and M. Arroyo. 2014. Importance of Force Decomposition for Local Stress Calculations in Biomembrane Molecular Simulations. Journal of chemical theory and computation 10:691-702.
5. Sodt, A. J., and R. W. Pastor. 2014. Molecular modeling of lipid membrane curvature induction by a peptide: more than simply shape. Biophysical journal 106:1958-1969.
6. Helfrich, W. 1973. Elastic properties of lipid bilayers: theory and possible experiments. Z Naturforsch C 28:693-703.
7. Sodt, A. J., R. M. Venable, E. Lyman, and R. W. Pastor. 2016. Nonadditive Compositional Curvature Energetics of Lipid Bilayers. Phys Rev Lett 117:138104.
8. Hess, B., C. Kutzner, D. van der Spoel, and E. Lindahl. 2008. GROMACS 4: Algorithms for Highly Efficient, Load-Balanced, and Scalable Molecular Simulation. Journal of chemical theory and computation 4:435-447.
9. Vuorela, T., A. Catte, P. S. Niemela, A. Hall, M. T. Hyvonen, S. J. Marrink, M. Karttunen, and I. Vattulainen. 2010. Role of lipids in spheroidal high density lipoproteins. PLoS Comput Biol 6:e1000964.
10. Bussi, G., D. Donadio, and M. Parrinello. 2007. Canonical sampling through velocity rescaling. J. Chem. Phys. 126:014101-014107.
11. Berendsen, H. J. C., J. P. M. Postma, A. DiNola, and J. R. Haak. 1984. Molecular dynamics with coupling to an external bath. J Chem Phys 81:3684-3690.
12. Shinoda, W., R. DeVane, and M. L. Klein. 2010. Zwitterionic lipid assemblies: molecular dynamics studies of monolayers, bilayers, and vesicles using a new coarse grain force field. The journal of physical chemistry. B 114:6836-6849.
13. MacDermaid, C. M., H. K. Kashyap, R. H. DeVane, W. Shinoda, J. B. Klauda, M. L. Klein, and G. Fiorin. 2015. Molecular dynamics simulations of cholesterol-rich membranes using a coarse-grained force field for cyclic alkanes. J Chem Phys 143:243144.
14. Shinoda, W., R. DeVane, and M. L. Klein. 2007. Multi-property fitting and parameterization of a coarse grained model for aqueous surfactants. Molecular Simulation 33:27-36.
15. Mitsche, Matthew A., and Donald M. Small. 2011. C-Terminus of Apolipoprotein A-I Removes Phospholipids from a Triolein/Phospholipids/Water Interface, but the N-Terminus Does Not: A Possible Mechanism for Nascent HDL Assembly. Biophysical journal 101:353-361.
16. Plimpton, S. 1995. Fast parallel algorithms for short-range molecular dynamics. Journal of computational physics 117:1-19.

17. Jo, S., J. B. Lim, J. B. Klauda, and W. Im. 2009. CHARMM-GUI Membrane Builder for mixed bilayers and its application to yeast membranes. Biophysical journal 97:50-58.
18. Nosé, S. 1984. A molecular dynamics method for simulations in the canonical ensemble. Molecular Physics 52:255-268.
19. Martyna, G. J., D. J. Tobias, and M. L. Klein. 1994. Constant pressure molecular dynamics algorithms. The Journal of Chemical Physics 101:4177-4189.
20. Parrinello, M., and A. Rahman. 1981. Polymorphic transitions in single crystals: A new molecular dynamics method. Journal of Applied Physics 52:7182-7190.
21. Eastwood, J. W., R. W. Hockney, and D. N. Lawrence. 1980. P3M3DP - THE 3-DIMENSIONAL PERIODIC PARTICLE-PARTICLE-PARTICLE-MESH PROGRAM. Computer Physics Communications 19:215-261.
22. Vamparys, L., R. Gautier, S. Vanni, W. F. Bennett, D. P. Tieleman, B. Antonny, C. Etchebest, and P. F. Fuchs. 2013. Conical lipids in flat bilayers induce packing defects similar to that induced by positive curvature. Biophysical journal 104:585-593.
23. Vanni, S., H. Hirose, H. Barelli, B. Antonny, and R. Gautier. 2014. A sub-nanometre view of how membrane curvature and composition modulate lipid packing and protein recruitment. Nature communications 5:4916.
24. Ding, W., M. Palaiokostas, W. Wang, and M. Orsi. 2015. Effects of Lipid Composition on Bilayer Membranes Quantified by All-Atom Molecular Dynamics. The Journal of Physical Chemistry B 119:15263-15274.

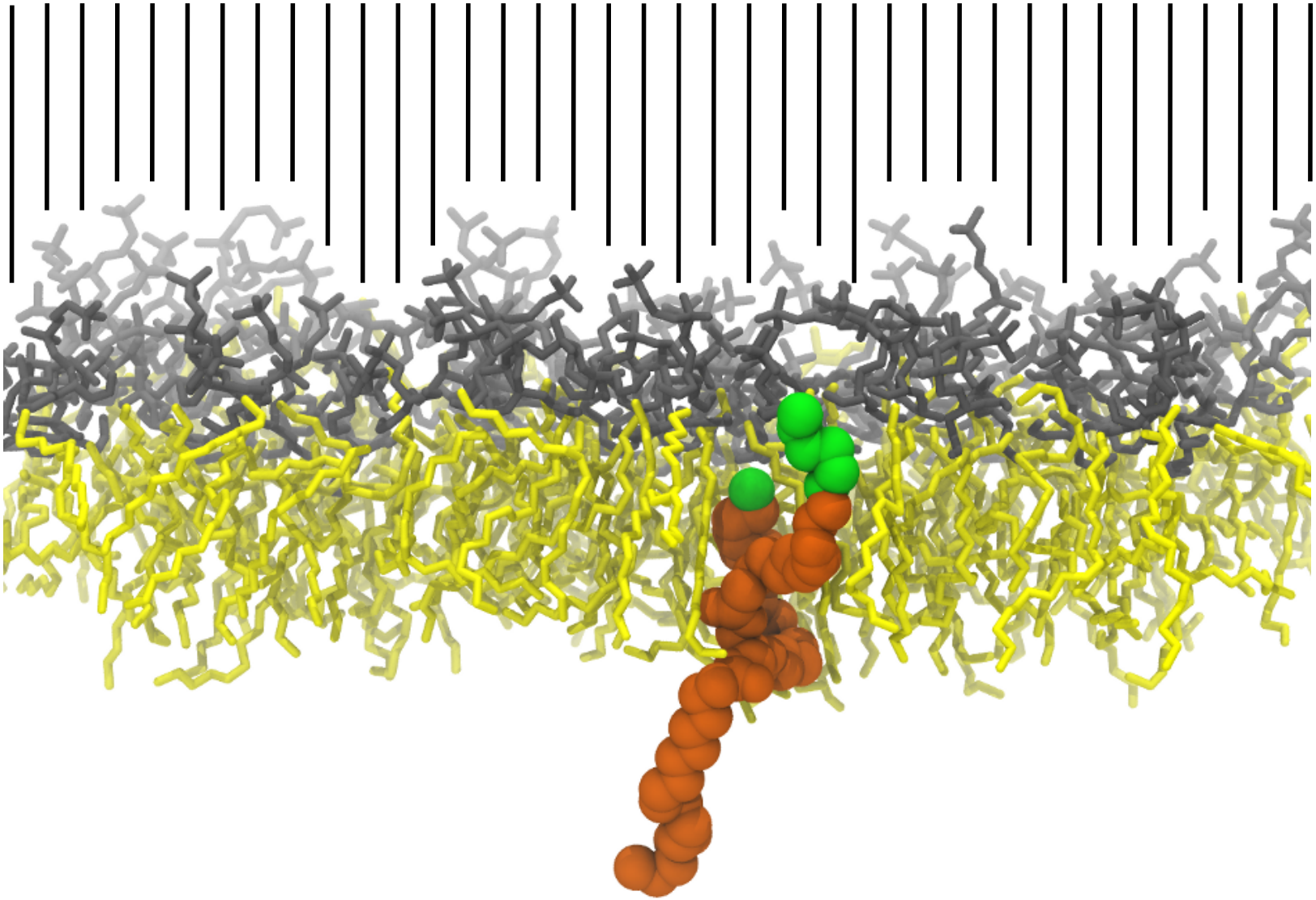

Figure S3. Packing defect analysis in the presence of triolein molecules. The polar head of the POPC are represented in grey, the apolar tails of the POPC are represented in yellow. The triolein in represented in orange spheres. The green spheres are the triolein atoms that are above the threshold of detection for the packing defect in the membrane.

a.

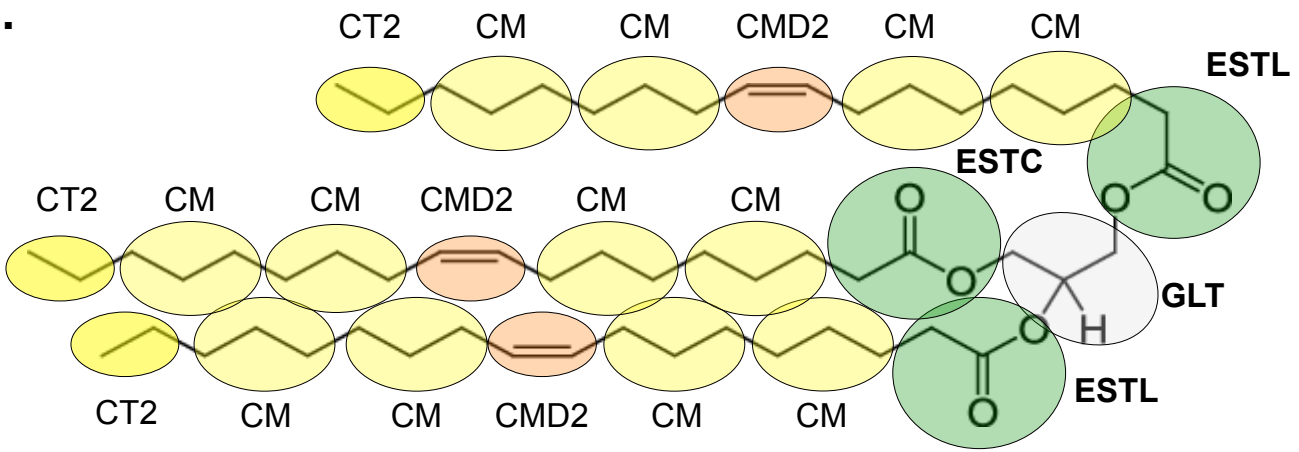

b.

Bonds	**k_b(kcal/mol/Å^2)**	**r_0 (Å)**
GLT ESTC	110.0	2.95
GLT ESTL	25	3.21
ESTC CM	8.0	3.70
ESTL CM	8.0	3.70
Angles	**k_θ (kcal/mol/rad^2)**	**θ_0 (deg)**
GLT ESTC CM	3.0	165
GLT ESTL CM	2.0	120
ESTC CM CM	1.3	180
ESTL CM CM	1.3	180
ESTC GLT ESTL	3.0	142
ESTL GLT ESTL	3.5	105
Pairs	**ε (kcal/mol)**	**σ (Å)**
GLT-W	0.26	4.4385

Figure S4. CG model for triolein (TO) based on the SDK procedure. a. AA to CG mapping. b. New bonded and non-bonded CG parameters involving TO beads.

pureTO	AA	CG-SDK mapped from UA						
		EST-C3	EST-C4	EST-C5	EST-C6	C1-C2	C1-C3	C1-C4
Trident	1.9	1	1.6	2.3	2.7	2.1	2.6	3.1
Chair	9.4	9.1	9.3	9.4	9.4	9.2	9.1	9.3
Fork	13.1	14.6	14	12.9	11.9	12.8	11.8	11.5
T	33.1	36.1	34.8	32.9	32.0	33.4	32.0	31.3
Hand	7.0	6.4	6.3	6.7	7.2	7.0	7.3	7.1
Stacker	21.3	18.3	19.8	21.6	22.7	21.4	23.1	23.6
Average abs error		1.6	0.9	0.2	0.8	0.2	0.9	1.2
Average rel error		15.6%	7.7%	4.8%	10.7%	2.7%	11.0%	15.7%

Table S5. Optimal bead selection to compute TO conformations using our TO CG model. TO conformations in UA simulations mapped to CG resolution using different beads to determine the chain vectors (see Methods). UA results are shown for comparison. EST: ester bead, C1-C6: acyl chain beads numbered from 1 (closer to the ester group) to 6 (terminal bead).

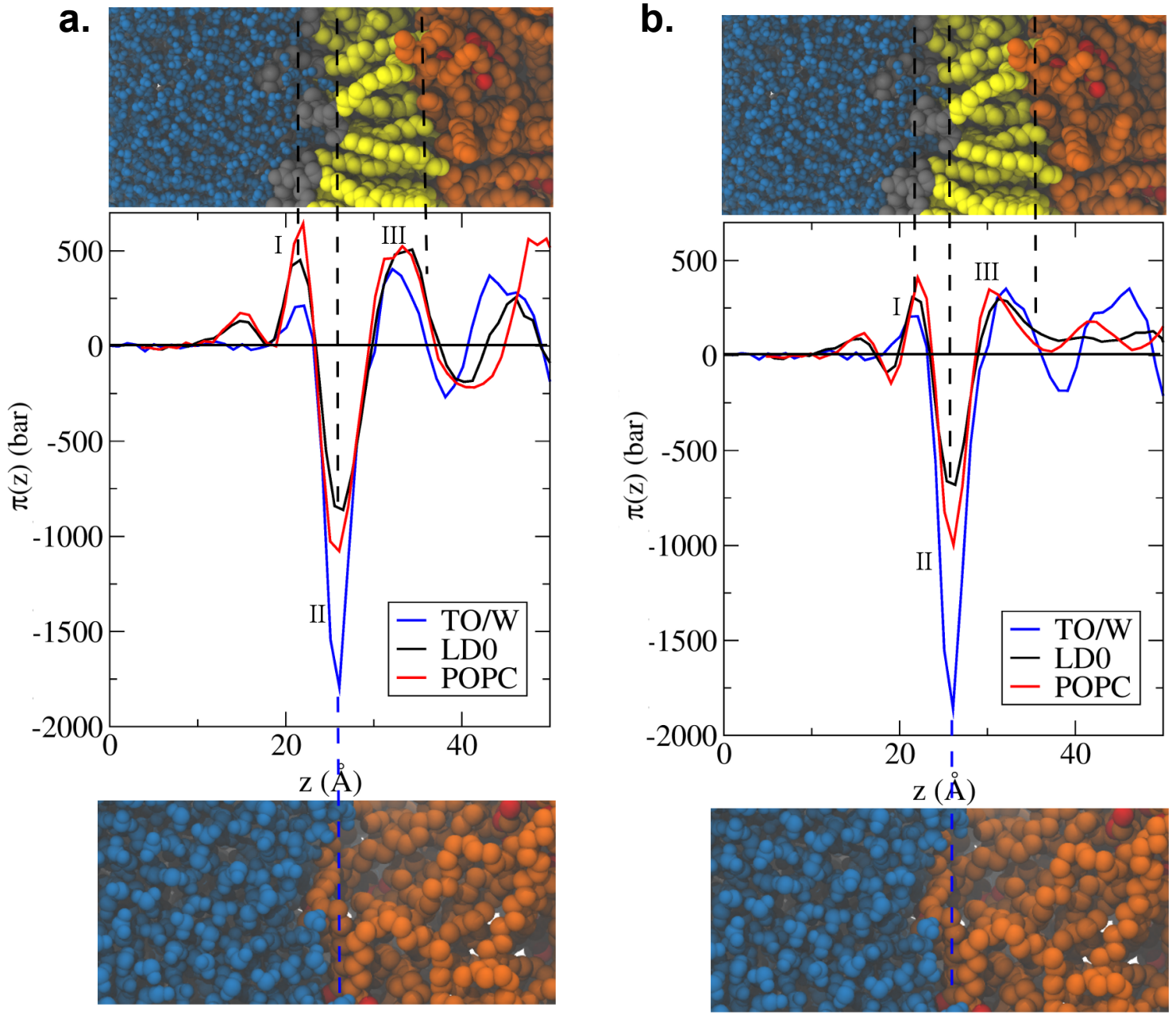

Figure S6. Comparison of the way of computing LPP in UA MD simulations. a. Central Force Decomposition (CFD). **b.** Goetz-Lipowsky Decomposition (GLD).

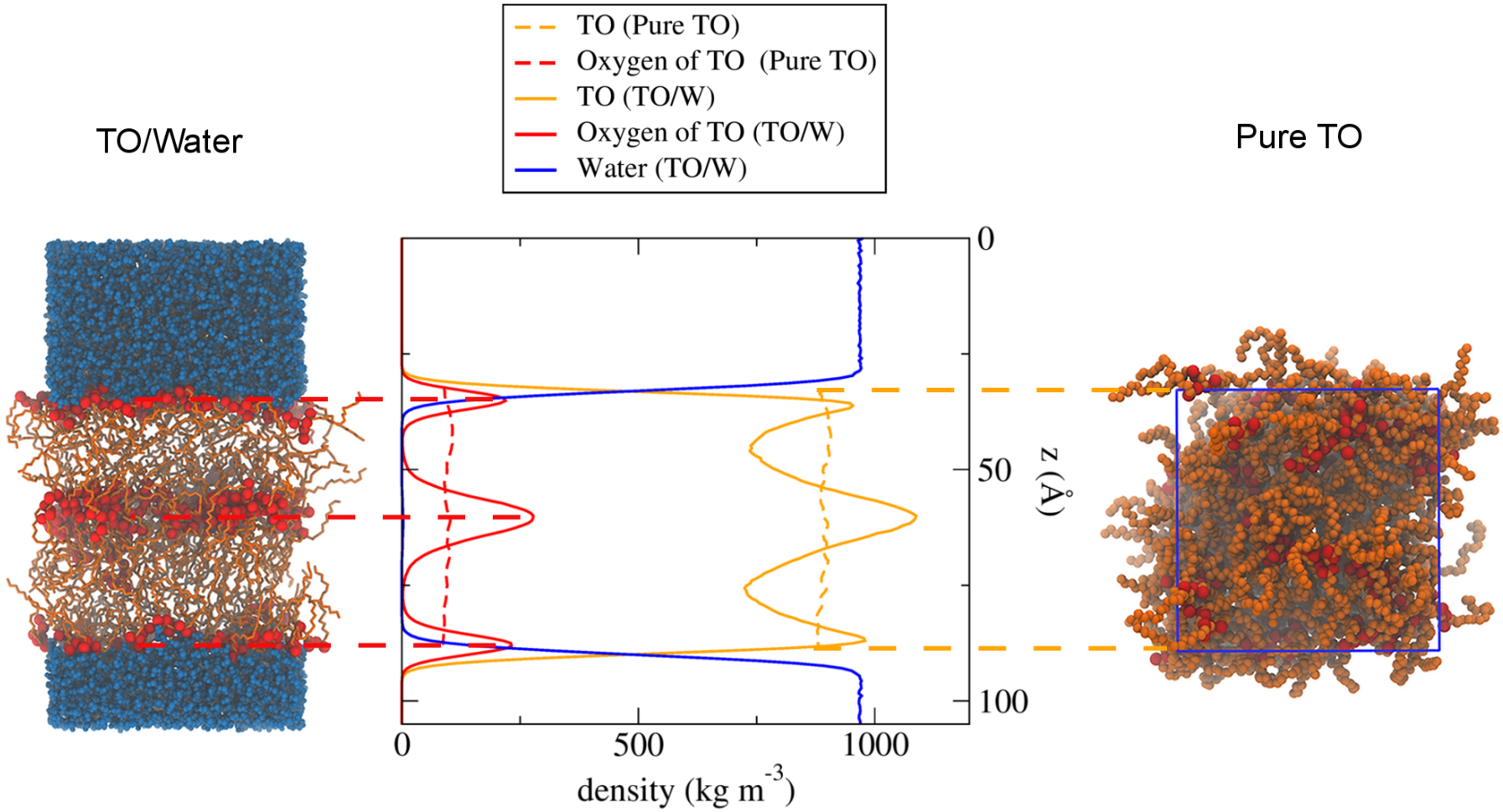

Figure S7. Density profiles of a pure triolein and of a triolein-water interface using UA MD simulations. Left: TO/W system. Right: Pure TO system. In the plot, continuous lines describe the pure triolein system, while dotted lines describe the TO/W system. The densities of the whole trioleins molecules are represented in orange and the oxygens are represented in red. In the triolein-water interface system, the oxygens are gathered and form 3 layers while there is such arrangement is absent in the pure triolein system, as shown by the flat lines.

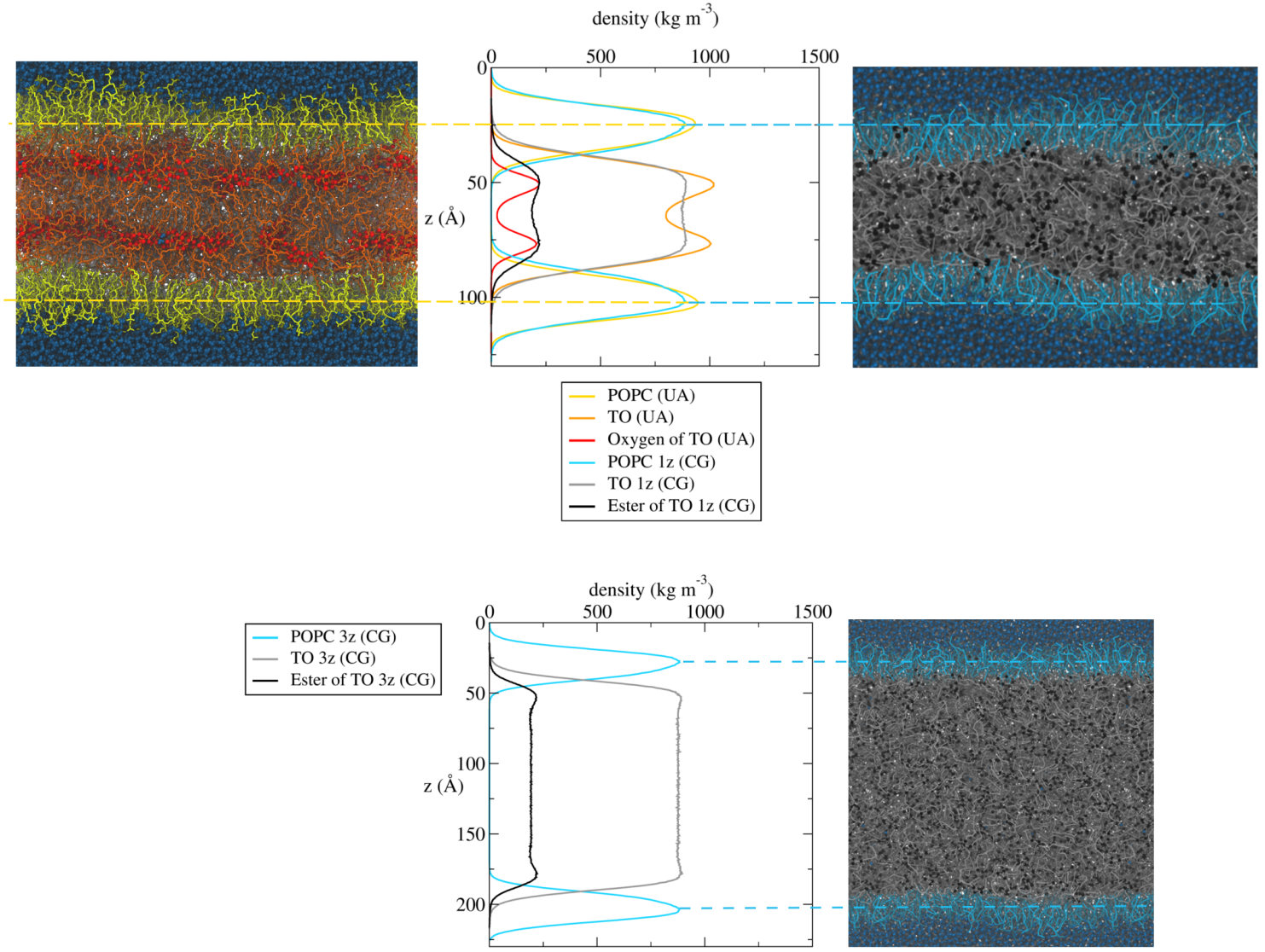

Figure S8. Comparison of triolein densities in united-atom system and coarse-grained systems using the CG-SDK forcefield with different triolein-core thicknesses. Left: united-atom LD snapshot: POPC are in yellow, TO in orange, oxygen atoms of TO in red spheres and water in blue spheres. Right: SDK CG LD snapshot: POPC are in cyan, TO in gray, oxygen atoms of TO in black and water in blue. The 1z system has a similar size as the UA system (top), the 3z system has the layer of oil that has been expanded 3 times in the z axis (bottom).

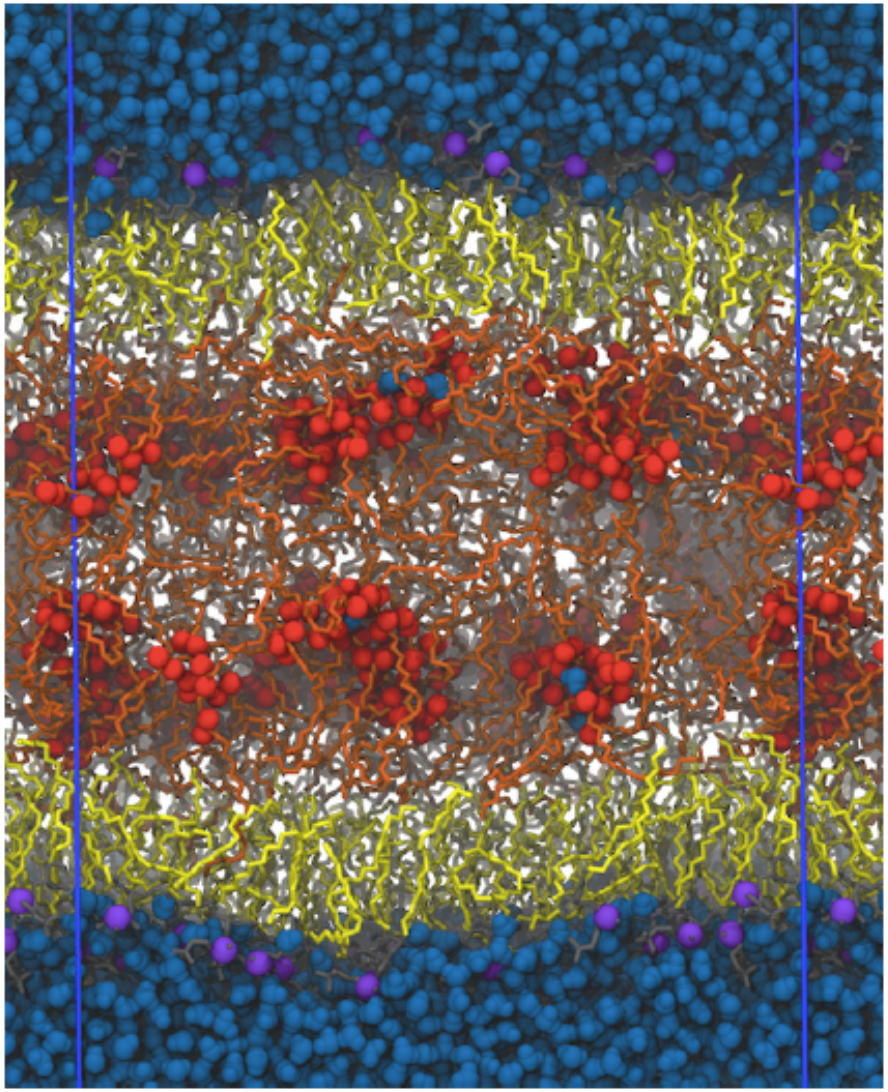

Figure S9. Snapshot of a LD0 system illustrating TO hydration using UA MD simulations. Same color coding as Figure 1 of the main article, except waters shown as spheres. Water molecules form hydrogen bonds with TO glycerol atoms.

	In	Out	In - Out
POPC bil			
MD #1	17	17	0
MD #2	25	25	0
LD 0%			
MD #1	29	17	12
MD #2	22	16	6
LD 1%			
MD #1	41	22	19
MD #2	27	15	12
LD 2%			
MD #1	38	22	16
MD #2	34	17	17
LD 5%			
MD #1	41	25	18
MD #2	30	21	9
LD 10%			
MD #1	129	118	11
MD #2	145	135	10
MD #3	79	68	11

Table S10. Hydration of the different systems in UA MD simulations. Number of water molecules entering (in) or leaving (out) the oily core of LD systems by crossing one POPC monolayer (upper or lower). The average net number of water residing in the oily phase (in - out) remain stable after 100 ns. For POPCbil, water molecules crossing a leaflet towards the bilayer center immediately leave (either crossing the same leaflet or the other one).

	Pure TO	TO/W	TO_Vac	LD				
				0 %	1 %	2 %	5 %	10 %
Trident	1.9	7.2 ± 0.1	1.8 ± 0.1	1.7 ± 0.1	1.9 ± 0.2	1.8 ± 0.1	1.8 ± 0.1	2.2 ± 0.1
Chair	9.4 ± 0.3	6.8 ± 0.1	11.0 ± 0.3	9.4 ± 0.7	10.1 ± 0.3	9.6 ± 0.5	9.7 ± 0.1	10.1 ± 0.5
Fork	13.1	9.4 ± 0.2	13.2 ± 0.1	14.2 ± 0.1	13.1 ± 0.6	13.4 ± 0.3	13.6 ± 0.1	13.6 ± 0.7
T	33.1	22.8 ± 0.3	32.2 ± 0.1	33.2 ± 0.3	32.2 ± 0.8	33.1 ± 0.3	33.1 ± 0.4	31.7 ± 0.6
Right Hand	7.0	7.8 ± 0.1	6.3 ± 0.1	6.7 ± 0.2	6.8 ± 0.1	6.9	6.8 ± 0.1	6.5 ± 0.2
Stacker	21.3	32.1 ± 0.3	21.4± 0.2	20.8 ± 0.6	21.8 ± 0.9	21.1 ± 0.4	20.9 ± 0.3	21.7 ± 0.5
Interface								
Trident		18.0 ± 0.3	2.8 ± 0.3					34.7 ± 3.7
Chair		1.4 ± 0.1	10.8 ± 0.3					0.4 ± 0.4
Fork		2.2 ± 0.1	9.1 ± 0.5					0.8 ± 0.7
T		7.6 ± 0.2	29.4 ± 0.5					3.4 ± 1.6
Right Hand		8.5 ± 0.1	7.6 ± 0.4					5.6 ± 1.9
Stacker		48.9 ± 0.6	26.1 ± 0.7					44.1 ± 4.3

Table S11. Conformational analysis of TO in the different systems using UA MD simulations. When errors are not reported, they are below 0.1. Interfacial values are not available for LD0, LD1, LD2 and LD5 since only few TO molecules per simulation reside in the interfacial region.

	Deep lipid-packing defect (Å^2)	Shallow lipid-packing defect (Å^2)	Surface Tension (mN m^{-1})
POPC bil			
MD #1	8.3 ± 0.2	9.8 ± 0.5	0.0
MD #2	8.3 ± 0.5	9.6 ± 0.6	0.0
LD 0%			
MD #1	9.6 ± 1.9	11.7 ± 0.8	0.0
MD #2	8.8 ± 1.1	10.0 ± 0.5	0.0
LD 1%			
MD #1	8.8 ± 0.9	11.6 ± 0.5	2.8 ± 1.2
MD #2	8.8 ± 0.4	11.2 ± 0.4	3.0 ± 0.5
LD 2%			
MD #1	9.0 ± 1.1	11.7 ± 0.2	5.5 ± 0.3
MD #2	8.5 ± 0.4	10.8 ± 0.7	5.2 ± 0.5
LD 5%			
MD #1	9.3 ± 0.7	12.4 ± 1.1	9.3 ± 0.3
MD #2	9.9 ± 0.7	12.4 ± 0.4	9.1 ± 0.2
LD 10%			
MD #1	10.8 ± 1.2	14.9 ± 1.5	12.0 ± 0.5
MD #2	11.2 ± 0.7	17.0 ± 0.6	12.4 ± 0.6
MD #3	10.2 ± 0.6	16.9 ± 1.3	12.8 ± 0.3

Table S12. Packing defect constants (in units of Å^2) compared to surface tension (in units of mN/m) in UA MD simulations. When the error is not indicated, it is below 0.1 mN/m

pureTO	UA	MARTINI
Trident	1.9	1.7
Chair	9.4	6.3
Fork	12.7	13.2
T	33.3	35.8
Hand	6.9	8.2
Stacker	21.4	20.5
Average abs error		1.4
Average rel error		12.2%

TO/W	UA	MARTINI
Trident	7.2	5.5
Chair	6.8	5.6
Fork	9.4	8.6
T	22.8	26.8
Hand	7.8	8.8
Stacker	32.1	30.4
Average abs error		1.7
Average rel error		14.2%

LD	UA	MARTINI
Trident	1.7	2.2
Chair	9.4	7.2
Fork	14.2	11.5
T	33.2	34.4
Hand	6.7	8.4
Stacker	20.8	1.7
Average abs error		1.6
Average rel error		14.8%

Table S13. TO conformations in MARTINI MD simulations. Left: liquid TO system. Center: TO – water interface. LD system. All systems have the same number of lipids than corresponding UA simulations.

pureTO	UA	SDK
Trident	1.9	1.8
Chair	9.4	9.3
Fork	12.7	9.7
T	33.3	34.9
Hand	6.9	8.5
Stacker	21.4	21.7
Average abs error		1.1
Average rel error		9.9%

TO/W	UA	SDK
Trident	7.2	8.7
Chair	6.8	5.7
Fork	9.4	5.9
T	22.8	22
Hand	7.8	8.5
Stacker	32.1	35.2
Average abs error		1.8
Average rel error		16.1%

LD	UA	SDK
Trident	1.7	2.0
Chair	9.4	9.2
Fork	14.2	9.8
T	33.2	34.2
Hand	6.7	8.4
Stacker	20.8	22.3
Average abs error		1.5
Average rel error		14.4%

Table S14. TO conformations in CG-SDK MD simulations. Left: liquid TO system. Center: TO – water interface. LD system. All systems have the same number of lipids than corresponding UA simulations.

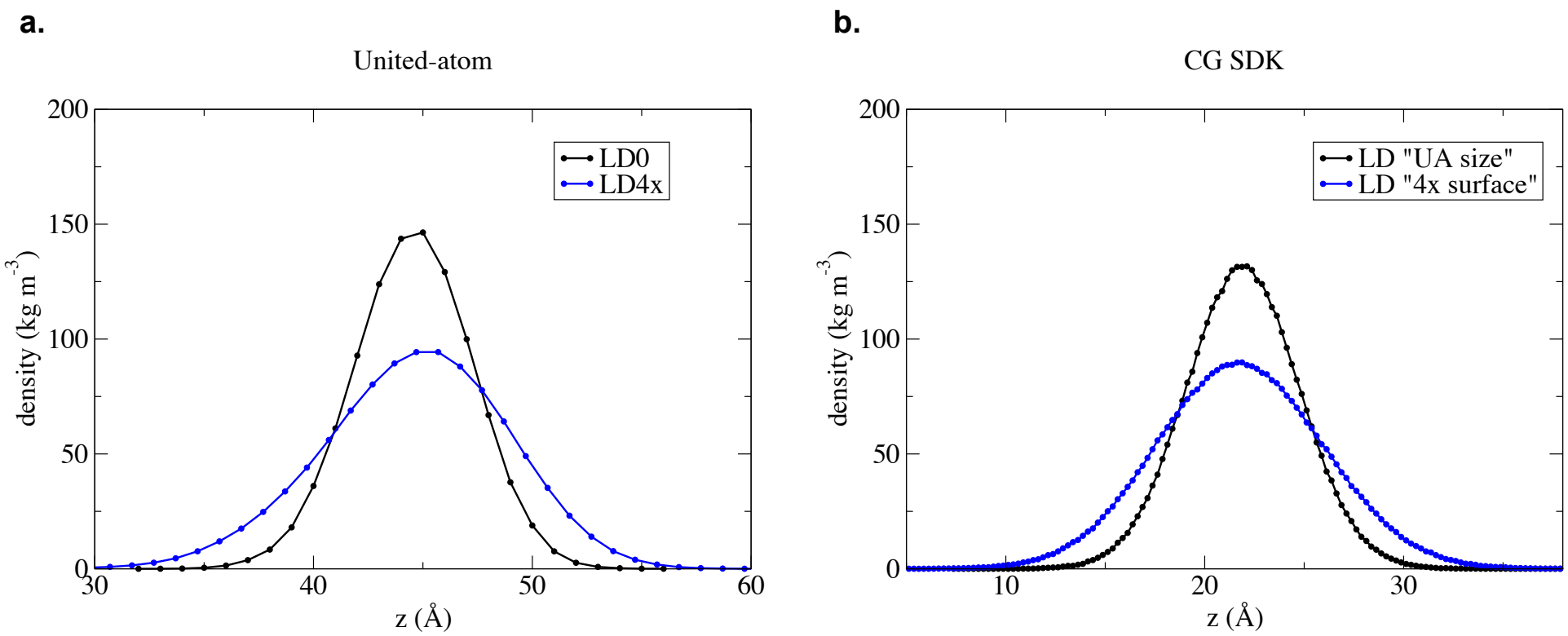

Figure S15. Fluctuations of the phosphate groups in UA and CG-SDK simulations as a function of lateral *(x,y)* system size. a. UA simulations. **b.** CG-SDK simulations.

Surface Tension (mN/m)	Whole system						Interface					
	Trident	*Chair*	*Fork*	*T*	*Hand*	*Stacker*	*Trident*	*Chair*	*Fork*	*T*	*Hand*	*Stacker*
0.2 ± 0.2	1.9	9.3	9.8	34.5	8.4	22	31.1	0.5	1.2	4.4	5.6	44.3
1.9 ± 0.2	1.9	9.2	9.7	34.6	8.4	22	29.1	1.4	0.8	4.2	5.6	44.5
4.7 ± 0.2	1.9	9.2	9.8	34.6	8.4	22	27.5	0.9	1.2	4.8	5.9	45.3
10.0 ± 0.2	2	9.2	9.7	34.4	8.4	22.1	24.9	1.1	1.4	5.9	6	47
16.0 ± 0.2	2.2	9.1	9.5	34	8.4	22.6	21.7	1.2	1.5	6.3	6.9	48.4
20.4 ± 0.1	2.5	8.9	9.4	33.5	8.4	23.3	20.6	1.4	1.5	7	7.3	48.4
26.1 ± 0.1	3.2	8.6	9	32.1	8.5	24.6	18.7	1.5	1.7	7.4	7.8	49
28.4 ± 0.1	3.8	8.2	8.6	30.9	8.5	25.9	18.3	1.5	1.7	7.5	7.9	49.2
32.0 ± 0.1	5.4	7.5	7.8	28.1	8.5	28.7	21.9	1	1	5.2	7.2	49.9

Table S16. TO conformations as a function of surface tension in CG-SDK simulations of model LDs. All conformation error bars are below 0.1. The last row represent the pure TO/W system in the absence of POPC molecules.